Southerly Surges on Submonthly Time Scales over the Eastern Indian Ocean during the Southern Hemisphere Winter

YOSHIKI FUKUTOMI

Frontier Research Center for Global Change, JAMSTEC, Yokohama, Japan

TETSUZO YASUNARI

Hydrospheric Atmospheric Research Center, Nagoya University, Nagoya, and Frontier Research Center for Global Change, JAMSTEC, Yokohama, Japan

(Manuscript received 5 June 2004, in final form 18 October 2004)

ABSTRACT

Meridional wind surges from the extratropics into the Tropics strongly regulate tropical convective activity. This paper confirms that extratropical forcing manifested as a meridional surge does modulate the tropical atmosphere over the eastern Indian Ocean, and it describes the tropical–extratropical connection in the region.

Surges in the lower atmosphere on submonthly (6–25 days) time scales over the eastern Indian Ocean were examined in tandem with associated tropical convection and large-scale atmospheric fields during the Southern Hemisphere (SH) winter (June–August). Data used in this study are NCEP-2 reanalyses and daily NOAA/Climate Diagnostics Center (CDC) outgoing longwave radiation (OLR) data for 23 yr, from 1979 to 2001. A low-level surge index was calculated using the 850-hPa meridional wind component (v) averaged over a region where sub–monthly scale v variance shows a local maximum (17.5°–2.5°S, 87.5°–97.5°E). The surge index defines 62 different surge events. Composites of various components were generated based on the index to define relationships between surge events and large-scale fields.

Low-level southerly surges over the eastern Indian Ocean originate from midlatitude Rossby waves with strong baroclinic development in the entrance region of a subtropical jet core off Australia's west coast. Strengthened low-level wind surges cause cross-equatorial flow stretching from the subtropical eastern Indian Ocean to the southern Bay of Bengal. Surges are accompanied by the advection of cold, dry air from midlatitudes into the Tropics. A cold and dry front develops at the leading surge edge during the surge period. Two to four days later, as the surge peaks, negative OLR anomalies develop near the key region. The OLR anomalies indicate a local blow up of convection over the tropical eastern Indian Ocean. Convection reflects increased instability in the surge region, which is caused by low-level dry air advection and near-surface moistening that is forced by enhanced sea surface evaporation associated with the surge. The southerly surge on submonthly time scales is an important bridge linking the Tropics and midlatitudes over the Indian Ocean.

1. Introduction

Meridional wind surges from the extratropics into the Tropics strongly regulate tropical convective activity. Over the last two decades, numerous studies have described the influence of cold surges on large-scale fields. These studies include pioneering works after the Winter Monsoon Experiment (WMONEX) in 1978–79, which established the fundamental relationships between the east Asian–North Pacific cold surges and convective activity over the tropical Pacific. Midlatitude wave propagation and cold surges have been shown to modulate tropical convective activity in the Asia–Pacific region during the Northern Hemisphere (NH) winter (e.g., Murakami and Sumi 1981; Pan and Zhou 1985; Kiladis et al. 1994; Meehl et al. 1996; Slingo 1998; Compo et al. 1999). These studies have shown that a high-frequency intraseasonal time scale shorter

Corresponding author address: Dr. Yoshiki Fukutomi, Frontier Research Center for Global Change, Yokohama Institute for Earth Sciences, Japan Agency for Marine-Earth Science and Technology (JAMSTEC), 3173-25 Showa-machi, Kanazawa-ku, Yokohama, Kanagawa 236-0001, Japan.
E-mail: fukutomi@jamstec.go.jp

than 30 days is a dominant time scale of tropical–extratropical interactions associated with east Asian cold surges. This time scale is conventionally called submonthly. Similar cold surges linking the Tropics and extratropics also occur over the eastern South Pacific and South America during the Southern Hemisphere (SH) winter and summer (e.g., Garreaud and Wallace 1998; Liebmann et al. 1999; Marengo et al. 2002).

A series of works by Murakami and collaborators (Murakami 1987; Wang and Murakami 1987; Shrestha and Murakami 1988; Murakami 1988a,b; Murakami and Sumathipala 1989) found low-level equatorward wind surges on a variety of spatial and temporal scales over the Indian Ocean and South Pacific. Their main focus was placed on lower-frequency intraseasonal time scales, the so-called Madden–Julian oscillation (MJO; Madden and Julian 1994) or a 30–60-day time scale, rather than higher-frequency time scales. In particular, the former four works showed strong southerly surges at 30–60-day time scales originating over the midlatitude Indian Ocean region that enhanced MJO-scale convection over south Asia. The latter two studies, Murakami (1988b) and Murakami and Sumathipala (1989), also investigated higher-frequency fluctuations such as the submonthly and synoptic time scales. These analyses showed that equatorward surges over the SH oceans coincided with transient westerly bursts and enhanced convection in equatorial regions. Notably, high-frequency equatorward surges will influence tropical circulation in purely oceanic regions. Unfortunately, their discussions were limited for the local relationships between the meridional surge and the westerly burst on these shorter time scales in the Tropics.

From a viewpoint of large-scale tropical–extratropical connection over the Indian Ocean, some important implications of extratropical forcing of tropical atmosphere were presented by also other authors. For example, Yasunari (1981a,b) suggested that the SH midlatitude westerly disturbance cause cold air penetration into the tropical Indian Ocean region, which can play a role in initiating cloud activity associated with the lower-frequency (30–40 days) oscillation of the Indian summer monsoon. On the other hand, Rodwell (1997) proposed the mechanism for a midlatitude injection that acts as the triggering of a break in Indian monsoon rainfall. His results, based on general circulation model experiments, showed that the injection of dry air produced by the SH midlatitude weather system occurs through the low-level cross-equatorial jet along the western flank of the Mascarene high and leads to dry conditions over India.

However, the structure and evolution of low-level wind surges at submonthly time scales over the Indian Ocean and their influence on larger scales have not been as well defined as the structure, evolution, and influence of equatorward surges over east Asia and the western Pacific, and over the South Atlantic and South America. The tropical–extratropical connection over the Indian Ocean at submonthly time scales remains poorly understood.

This study examines the structure and evolution of low-level southerly surges and their influence on large-scale circulations and convective activities over the Indian Ocean on submonthly time scales. A preferred location for an equatorward low-level wind surge will be identified for the SH winter, and a cause–effect relationship will be established between the surge, the tropical atmospheric conditions, and the midlatitude systems in the location. During the SH winter, midlatitude disturbances at this high-frequency range favorably propagate along comparatively lower latitudes that correspond to the region of the SH subtropical jet (e.g., Ambrizzi et al. 1995; Kiladis and Mo 1999). Thus, a close connection between the midlatitude systems and tropical variability can be expected also over the Indian Ocean. The purpose of the present study is to confirm that sub–monthly scale extratropical wave forcing manifested as a meridional surge modulates the tropical atmosphere and to establish an associated tropical–extratropical connection over the Indian Ocean during the SH winter.

Data sources and the analysis procedures for this paper are described in section 2. Section 3 includes a statistical analysis that defines the basic characteristics of the sub–monthly scale surge activity at a low level in the atmosphere. In section 4, composite analysis results describe the space–time evolution of the large-scale fields associated with the surge. Section 5 then shows evidence of the possible impacts of the surge on the tropical atmosphere. Surge characteristics and related aspects are discussed in section 6, followed by conclusions in section 7.

2. Datasets and processing

Two datasets were used in this study to characterize the large-scale aspects of atmospheric circulation and convection associated with low-level wind surges. The National Centers for Environmental Prediction (NCEP)–Department of Energy (DOE) Atmospheric Model Intercomparison Project (AMIP-II) reanalysis (hereafter R2) dataset (Kanamitsu et al. 2002) includes zonal and meridional wind components (u, v), temperature (T), specific humidity (q), sea level pressure (SLP), geopotential height (Z), and surface latent and sensible heat fluxes (LHF and SHF). An interpolated outgoing long-

wave radiation (OLR) dataset provided by the National Oceanic and Atmospheric Administration (NOAA)/Climate Diagnostics Center (CDC) was also used. All data records include daily averages for the 23-yr period (1979–2001) at global coverage on a 2.5° latitude–longitude grid. In addition, streamfunction (ψ), relative vorticity (ζ), and divergence (Div) were computed from the R2 winds using a spherical harmonic transform (SPHEREPACK 3.0; Adams and Swarztrauber 1999). Potential vorticity (PV) on an isentropic surface was calculated from relative vorticity and temperature in three dimensions using the method described in Tomas and Webster (1994).

Both filtered and unfiltered anomalous time series at each grid point capture the space–time structure of the large-scale fields. Unfiltered daily perturbations of the variables were computed by removing the 23-yr climatological seasonal cycle from the raw 365-day time series for each year. The climatological seasonal cycle is defined as the sum of the 23-yr mean and the first three harmonics of the daily climatological mean values at each grid point. Submonthly (6–25-day) perturbations were computed by applying a Butterworth filter (Kaylor 1977) to the unfiltered perturbations. This bandpass filter has a sharp cutoff and effectively reduces the effect of both higher-frequency (synoptic) and lower-frequency intraseasonal (MJO or about 30–60-day band) fluctuations. The focus of this study is the SH winter; analysis results are given for the SH winter season, 1 June through 31 August [June–July–August (JJA)]. The reason is that significant extratropical–tropical connections are expected associated with disturbance activity embedded in the SH midlatitude westerly flow during this season, as noted in section 1.

3. Surge activity over the Indian Ocean

a. Sub–monthly scale surge and transient eddy activity

Figure 1 illustrates general features of variability at submonthly time scales in the target region. Three variance statistics products are given for JJA. Daily 850-hPa v is a key measure of low-level surge activity. Figure 1a shows the geographical distribution of variance for the 6–25-day filtered v at 850 hPa and its percentage of subseasonal total variance of unfiltered v. Local maximum values of variance exceeding 4 $m^2 s^{-2}$ overlap the ratio exceeding 45% over the tropical eastern Indian Ocean southwest of Sumatra. This high variability can be viewed as low-level meridional surge activity. The box (17.5°–2.5°S, 87.5°–97.5°E) enclosing this local maximum shows the key region (outlined in the figures) used for making a surge index to construct composites of various elements shown later. The surge index is defined from the average of the 6–25-day filtered 850-hPa v time series over this key region. The variance and percentage variance of the 6–25-day filtered OLR, as in Vincent et al. (1998), are also presented in Fig. 1b to confirm the sub–monthly scale convective activity. Comparatively high values, up to 700 $W^2 m^{-4}$, are located in the surge key region, which suggests a possible relationship between tropical convection and surge activity over the tropical eastern Indian Ocean. Disturbance activity in the upper troposphere is commonly measured by the perturbation (eddy) kinetic energy (PKE) (e.g., Matthews and Kiladis 1999). Here, PKE is derived from the 6–25-day filtered eddy components of u and v, that is,

$$\mathrm{PKE} = \frac{1}{2}(\overline{u'^2 + v'^2}), \tag{1}$$

where the overbar denotes the time mean, and the prime is the eddy component. The PKE is displayed with the SH winter-mean u component (Fig. 1c). The most striking feature is a band of maximum PKE exceeding 70 $m^2 s^{-2}$ that extends along the winter-mean subtropical jet from the Indian Ocean through the South Pacific. Sub–monthly scale eddy activities are most amplified near the subtropical jet core during the SH winter, which is consistent with Rossby wave activities with similar SH winter time scales investigated by Ambrizzi et al. (1995).

b. Surge index characteristics

Figure 2a shows the ensemble power spectrum of the unfiltered time series of 850-hPa v averaged over the surge key region for the 23 winters. Meridional surge activity over the eastern Indian Ocean has a dominant submonthly time scale. A fast Fourier transform (FFT) method estimated the power spectra for 128 days (14 May–18 September) centered on each individual winter (JJA, 92 days). A 99.9% significant peak at 14.4 days and associated larger power in submonthly ranges are clearly evident. In the winter of 2000 (Fig. 2b), a significant peak and its associated prominent power occur in the submonthly frequency range. Results in Fig. 2 support the existence of surges at submonthly scales and justify applying a bandpass filter to the time series. Figure 2c shows the 6–25-day filtered and unfiltered surge indices during JJA 2000, an unfiltered time series that corresponds to the power spectrum in Fig. 2b. These two time series are very similar; the 6–25-day filtered series is used as the southerly surge index to composite fields. Quasi-periodic, low-level wind

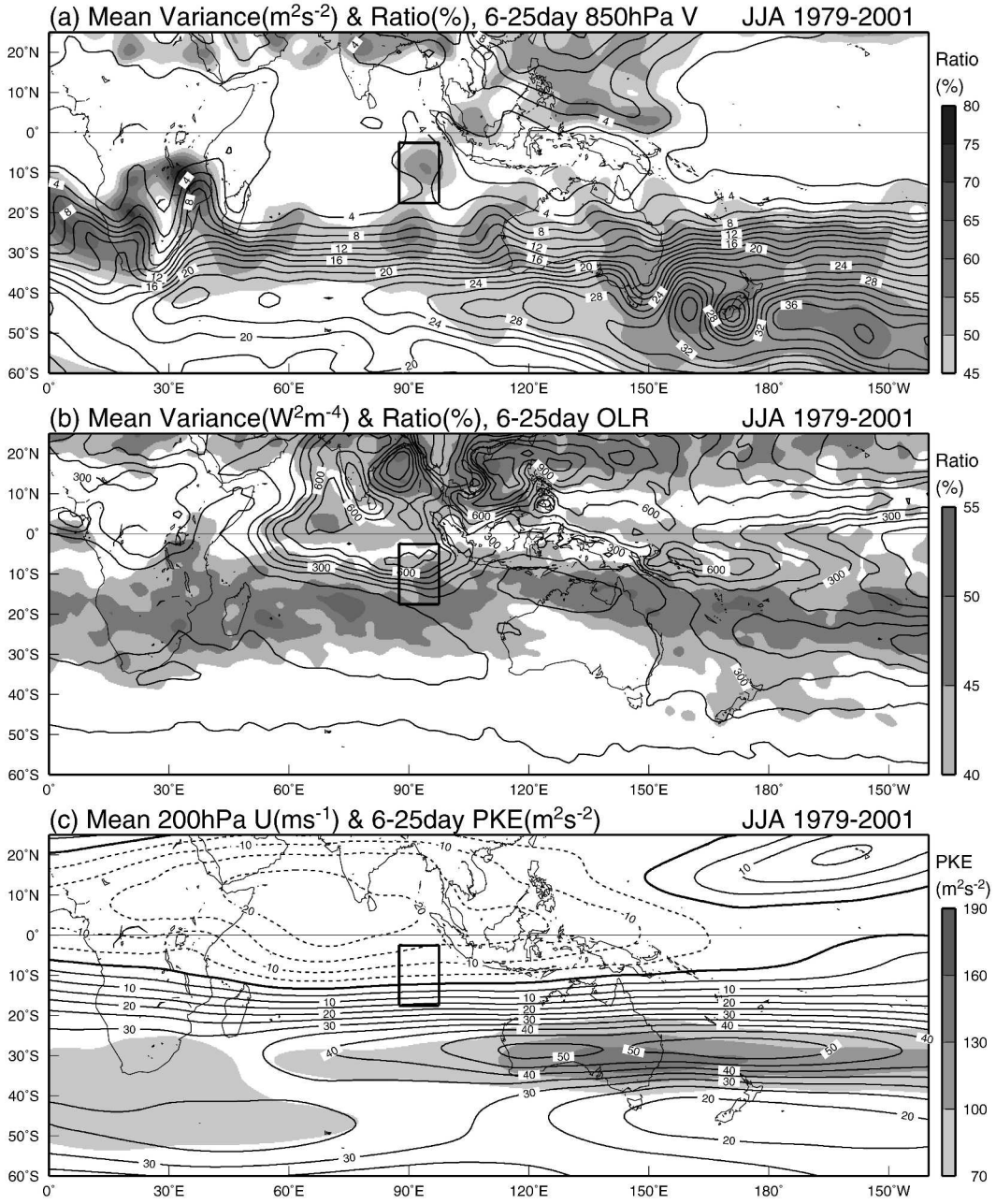

FIG. 1. (a) Variance of 6–25-day filtered meridional wind at the 850-hPa level (contours) and its percentage of total variance (shadings) for JJA (SH winter) 1979–2001. Contour interval is 2 $m^2 s^{-2}$. The surge key region is enclosed by the grid box of 17.5°–2.5°S, 87.5°–97.5°E. (b) Same as (a) except for OLR. Contour interval is 100 $W^2 m^{-4}$. (c) Mean zonal wind (contours) and 6–25-day PKE (shadings) at the 200-hPa level during the same period. Thin solid (dashed) contours indicate positive (negative) values. Thick solid contours are 0 values. Contour interval is 5 $m^2 s^{-2}$.

maxima occur with approximately 10- to 20-day periods in the time series. Positive extrema (denoted by inverted triangles) that exceed climatology by 1.5 standard deviations were selected as southerly surge peaks. Further details of the compositing technique are included below.

4. Space–time evolution of southerly surges and large-scale fields

a. Composite method

In this section, compositing techniques are used to establish relationships between southerly surges and

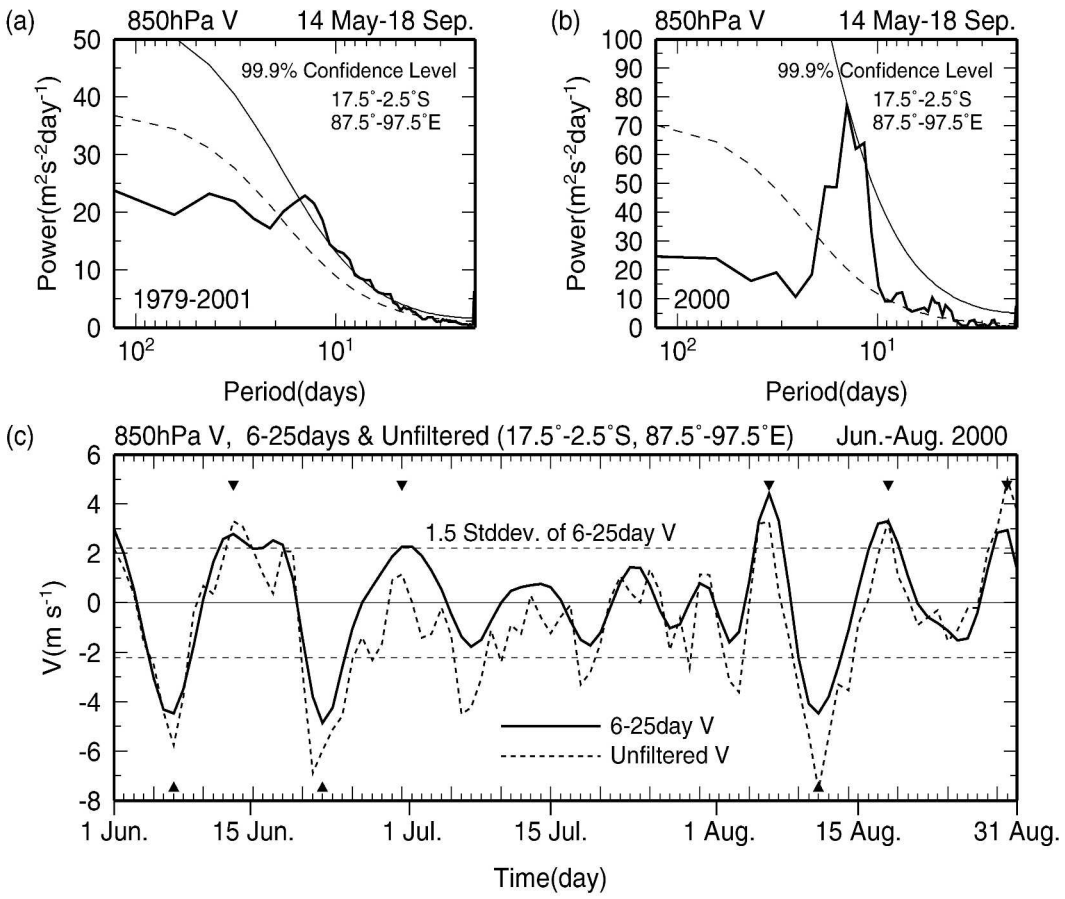

FIG. 2. (a) The 23-winter ensemble power spectrum of 850-hPa meridional wind averaged over the surge key region. Thin solid curve is the 99.9% confidence level. Dashed curve is the red noise spectrum. (b) Same as (a) except for 2000 winter case. (c) The 6–25-day filtered (thick solid line) and unfiltered (thick dashed line) 850-hPa meridional wind time series over the surge key region (surge index) for JJA 2000; 23-winter climatological 1.5 std dev (thin dashed lines), surge peaks (reversed triangles), and antisurge peaks (triangles) are also shown.

large-scale atmospheric conditions. Southerly surge peaks, as displayed in Fig. 2c, are referred to as day-0 phases; daily lag composites for various elements for day −5 through day +5 are constructed. A total of 62 surge events were identified during the 23 SH winter seasons, and space–time composites were defined by both filtered and unfiltered anomalies. A Student's *t*-statistic procedure (two-tailed *t* test) for the two-sample case determined the local statistical significance of the composites. The procedure is almost identical to that in Murakami (1987) and requires composite mean differences between paired reversal phases at each time stage. To do this in the present study, a total of 58 negative surge index peaks (as shown by triangles in Fig. 2c) were detected, and the composite differences between the positive and negative surges were tested for statistical significance. Additionally, critical values for area significance were determined from Monte Carlo experiments to confirm spatial significance of the composite maps (cf. Murakami 1987). Then, the spatial significance of the composite patterns was tested using these critical values.

b. Horizontal structure of southerly surge

Figure 3 shows the horizontal flow structure of the low-level surge at 850 hPa. Left panels (Figs. 3a–c) show composites of total wind vectors and the meridional wind component (v: shading and contour) for days −3, 0, and +3. At day 0, southeasterly–southerly flow penetrates from the SH subtropics into the southern Bay of Bengal over the eastern Indian Ocean. This surge flow converges with Asian monsoon westerly flow that extends from the Arabian Sea to the Philippines. The meridional surge flowing into the NH is not present 3 days before and after the peak surge.

Right panels (Figs. 3d–f) show similar composites with unfiltered v anomalies. Unfiltered anomalies were

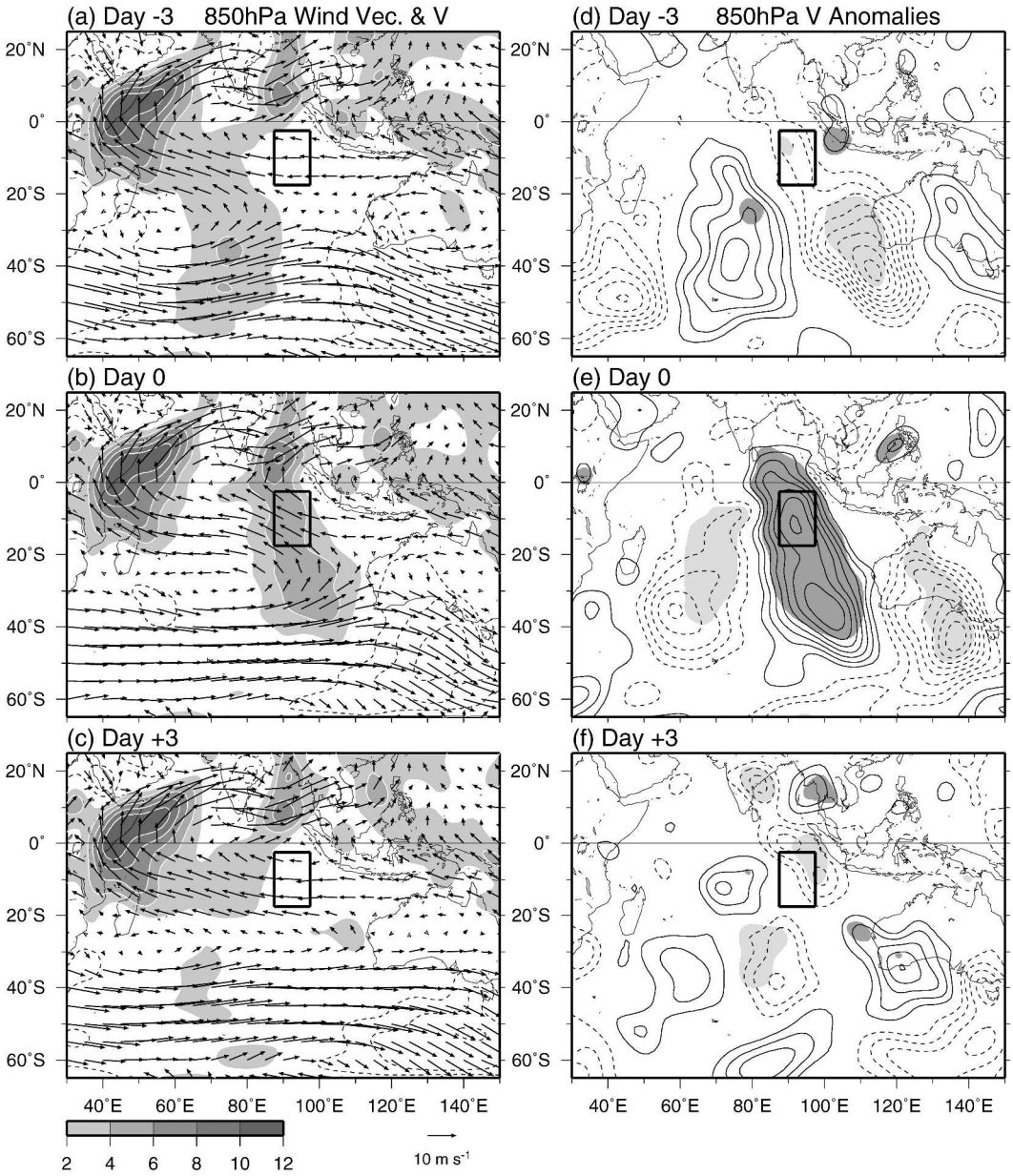

FIG. 3. (a)–(c) Composites of 850-hPa total wind vectors and meridional wind component (shadings and dashed contours) at day −3, day 0, and day +3 based on the surge index. Positive (negative) values are shadings (contours), and 0 values are omitted. Contour interval is 2 m^{-1}. (d)–(f) Composites of unfiltered meridional wind anomalies at the same timing. Solid (dashed) contours are positive (negative) values. Contour interval is 0.5 m s^{-1}. Positive (negative) anomalies statistically significant at the 99.9% level are darkly (lightly) shaded.

computed by subtracting the seasonal cycle as noted in section 2. An east–west-oriented wave pattern of v anomalies and a clear penetration of a positive v (southerly) anomaly into the southern Bay of Bengal is evident on day 0. The positive v anomaly propagates eastward across the Indian Ocean from day −4 through day +2 (not shown) and decays by day +3.

Composites of the 6–25-day filtered v anomalies (not shown) show patterns similar to those of the unfiltered anomalies. The eastward-propagating v anomalies contribute an oscillating off–on–off structure to the cross-equatorial flow that connects the SH midlatitude westerly flow to the NH monsoon westerly flow in the lower troposphere. These quasi-periodic surges over the eastern Indian Ocean might play an important role in meridional airmass exchange between the two hemi-

spheres, as is shown in the case of the east Asian winter monsoon surge by Carrera and Gyakum (2003).

c. Midlatitude waves and tropical convection

The eastward propagation of low-level v anomalies (Figs. 3d–f) suggests that midlatitude waves induce equatorward surges over the eastern Indian Ocean. In addition, the low-level surges can alter the tropical atmospheric condition, which may lead the occurrence of tropical convection. The evolution in space and time for the broader domain of the large-scale circulation and the convection associated with surges are presented here to capture the cause and effect of southerly surges.

Figure 4 illustrates the relationships between the southerly surges, low-level circulation, and convective activity using composite maps of the 6–25-day filtered 850-hPa wind vectors, streamfunction, and OLR anomalies every 2 days from day −2 to day +4. Composite wind vectors were tested statistically, and only those vectors for which the u or v component exceeded the 95% confidence level were plotted. In addition, OLR values less than -5 W m^{-2} were shaded.

From day −2 through day +2, a wave with cyclonic and anticyclonic circulation anomalies propagates along midlatitudes from the southwestern Indian Ocean into the South Pacific. This wave appears to produce the southerly surge flow as it amplifies. At day −2 (Fig. 4a), a wave train extends from south of Africa to south of Australia. Southwesterly and southerly wind anomalies, which are an early surge stage, appear in the key region; these wind anomalies originate from the midlatitude wave train.

At day 0 (Fig. 4b), the surge peaks when strengthened southerly winds cross the equator and reach the southern Bay of Bengal as part of a meridionally elongated trough–ridge couplet over the Indian Ocean. The midlatitude wave train that includes this trough–ridge couplet is well organized at day 0. Two days after the peak (day +2; Fig. 4c), the anomalous surge flow maintains its strength, but the direction shifts from southerly to southeasterly in association with the eastward traveling midlatitude trough–ridge pair. At the same time, a negative OLR anomaly begins to spread over the eastern equatorial Indian Ocean west of Indonesia.

By day +4 (Fig. 4d), the wave train and the southerly surge have decayed, but the negative OLR anomaly reaches a maximum over the key region. This OLR signal reflects enhanced convection that is likely triggered by the surge. The location of the OLR anomaly is consistent with that of the local maximum of OLR variance in the surge key region (Fig. 1b). The strengthened southerly surge could create favorable atmospheric conditions for local convective development in the key region. The surge-related change in the tropical atmosphere is discussed in section 5.

Another notable feature in the composite fields is the westward propagation of low-level westerly wind anomalies north of the equator. Between days −2 and +4, significant westerly winds propagate westward from the South China Sea to the Arabian Sea between 5° and 15°N. The westerly wind signal is on the southern flank of an anomalous cyclonic circulation that is associated with negative OLR anomalies. This westward-moving disturbance may be similar to those discussed by Fukutomi and Yasunari (1999, 2002). In addition, the confluence of the cross-equatorial southerly surge flow and the monsoon westerly flow at day 0 in the anomaly map (Fig. 4b) coincides with the flow in the total wind map (Fig. 3b). Development of low-level westerly winds over the Bay of Bengal is coincident with cross-equatorial southerly flow. This is similar to the relationships between the east Asian cold surge and subsequent development of transient westerly wind bursts over the western Pacific (e.g., Murakami and Sumathipala 1989; Kiladis et al. 1994; Meehl et al. 1996; Compo et al. 1999).

The behavior of the upper-level circulation associated with the evolving low-level surge was investigated to clarify the connection between the surge and midlatitude wave development. Figure 5 shows composite anomalies of 6–25-day filtered 200-hPa wind vectors, streamfunction, and OLR, similar to those in Fig. 4. However, OLR anomalies are mapped only for regions with 99.9% statistical significance, and negative (positive) anomalies are darkly (lightly) shaded.

The composite sequence shows a wave train that stretches from the southern Indian Ocean to the South Pacific, with eastward propagating wave anomalies and wave packets. The dominant zonal wavenumbers are 5–7. As the wave packet moves eastward across Australia during the surge period (day −2 through day +2), the wave anomalies grow downstream, suggesting Rossby wave energy propagation to the east. An arc of anticyclonic and cyclonic circulation centers curving toward the equator is nearly superposed on the JJA mean subtropical jet over the eastern Indian Ocean, Australia, and the South Pacific (Fig. 1c). At the surge peak (day 0; Fig. 5b), an amplified trough–ridge couplet over the eastern Indian Ocean shifts westward about 10° relative to corresponding features at 850 hPa; this structure is consistent with a baroclinic midlatitude wave. The low-level southerly surge could therefore be related to baroclinic development of the eastward-propagating wave in the entrance region of the SH subtropical westerly jet core over the eastern Indian Ocean. This is analogous to the east Asian cold surge that oc-

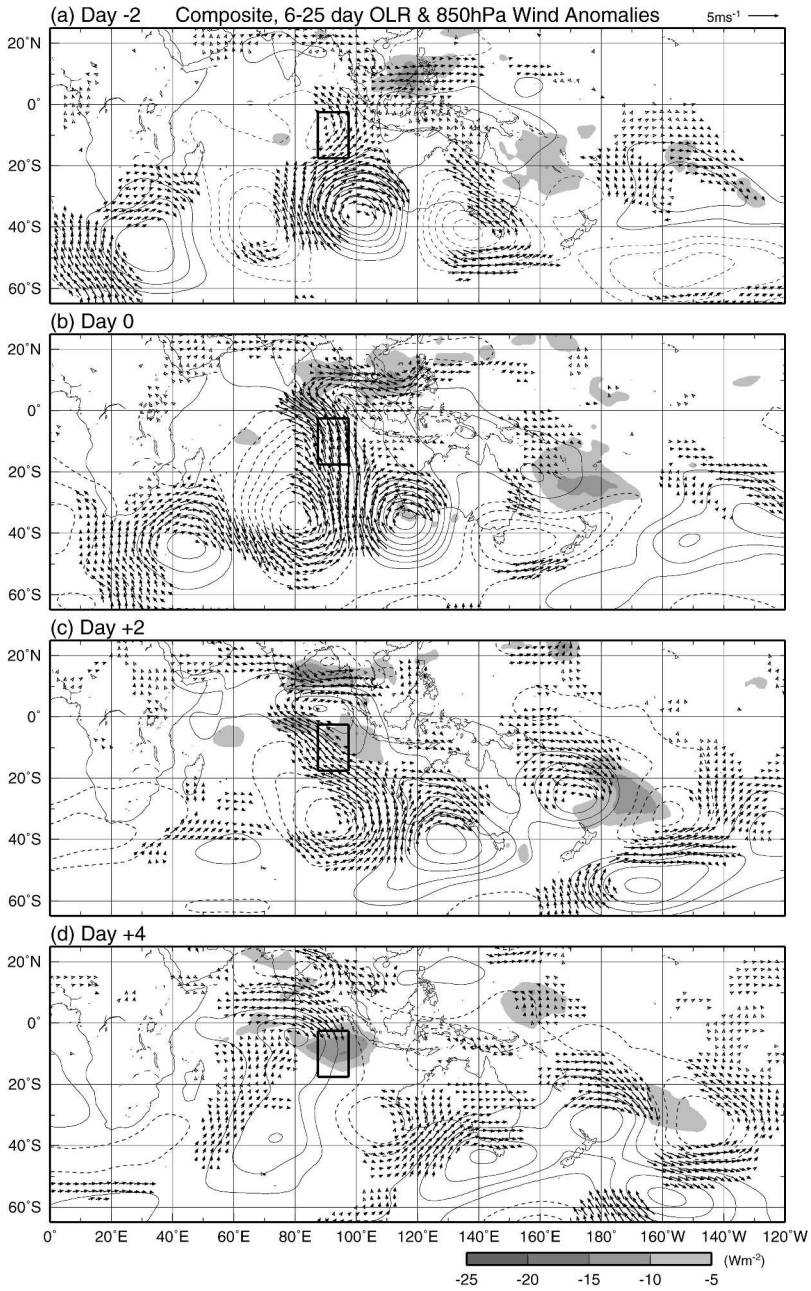

FIG. 4. Composites of 6–25-day filtered OLR, 850-hPa wind vectors and streamfunction anomalies from day −2 through day +4 with 2-day interval based on the surge index. OLR anomalies less than −5 W m^{-2} are shaded. Solid (dashed) contours are positive (negative) streamfunction values. Zero contours are omitted. Contour interval is 5.0×10^5 m^2 s^{-1}. Only 95% statistically significant vectors are plotted.

curs in the entrance region of the Asian–Pacific subtropical jet during the NH winter as illustrated with a conceptual model by Slingo (1998). At the mature stage of convection in the key region (day +4), the wave train weakens, but it still maintains the arc-like structure with new anticyclonic circulation growth at its leading edge over the South Pacific.

Characteristics of the upper-level waves in the present study agree with those in Ambrizzi et al. (1995). The motion of the anomalous troughs and ridges of the wave train (Fig. 5) is controlled by a waveguide along the subtropical and subpolar westerly jets for the SH winter. The waves follow an interesting route in the present case. The wave pattern moves northeastward

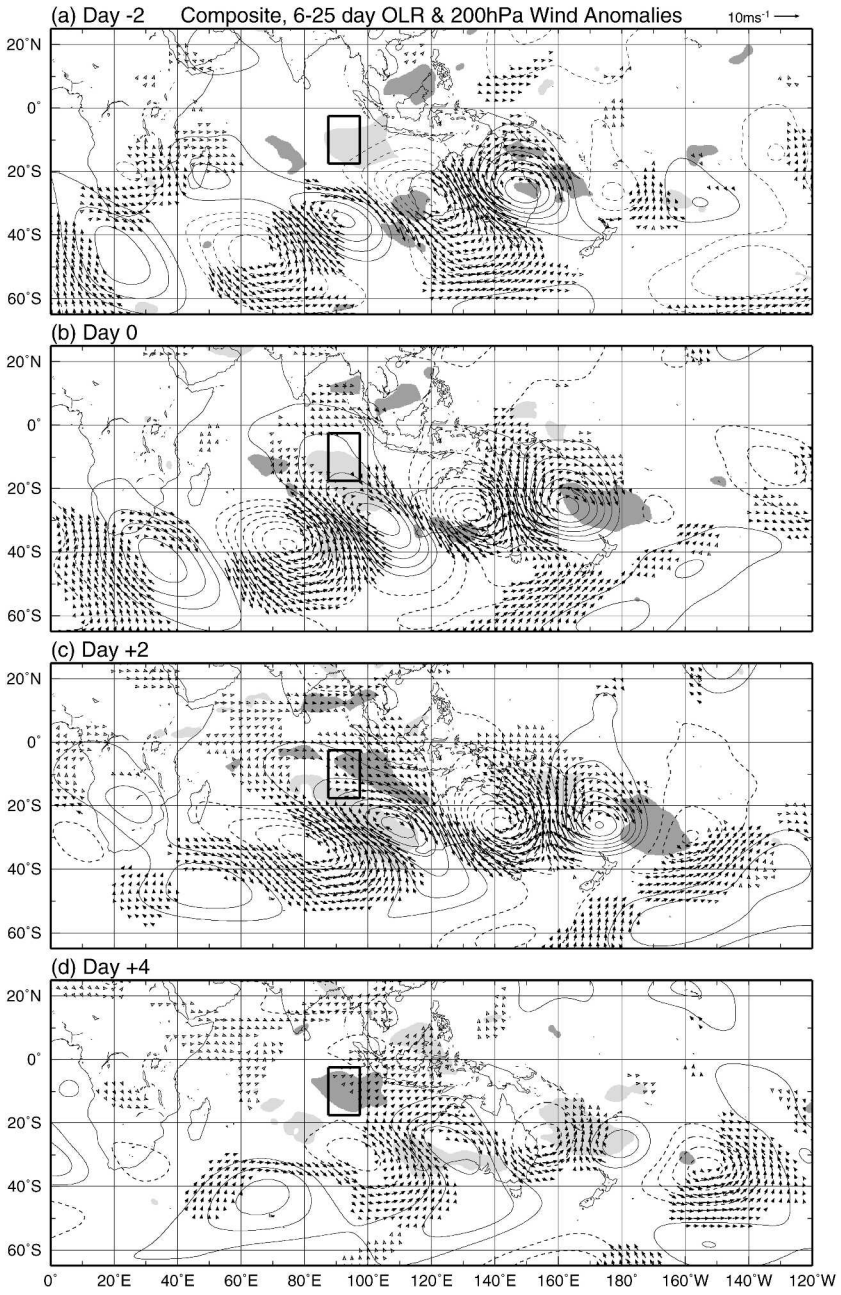

FIG. 5. Same as Fig. 4 except for 200-hPa wind fields and 99.9% statistically significant OLR anomalies. Contour interval is 1.0×10^6 m^2 s^{-1}. Negative (positive) OLR anomalies statistically significant at the 99.9% level are darkly (lightly) shaded.

into the Tropics on the upstream side over the Indian Ocean and the Australian continent; it then moves southeastward into midlatitudes on the downstream side over the South Pacific. The turning point for the waves is over the Coral Sea east of Australia (near 20°S, 165°E). Overall, the behavior of waves in the composite sequence is consistent with waves trapped inside the SH winter waveguide and reflected at a critical line at the boundary between the subtropical westerlies and tropical easterlies near 10°N (Fig. 1c).

Significant negative OLR anomalies that are associated with the leading edge of the southwest–northeast-oriented upper-level wave train develop in the subtropical South Pacific. From day −2 through day +2, OLR anomalies ahead of a trough east of Australia expand eastward as the wave train propagates down-

stream. This OLR signal represents convective activity at submonthly scales in the South Pacific convergence zone (SPCZ) region in conjunction with the midlatitude wave activity (e.g., Schrage and Vincent 1996).

5. Impacts of the southerly surge on the tropical atmosphere

a. Cold and dry air advection from midlatitudes into the Tropics

Basic circulation structures and convective signatures associated with low-level southerly surges have been identified. Figure 6 shows a sequence of 925-mb temperature and specific humidity anomaly composites to elucidate changes in the tropical lower-troposphere conditions during surges.

Composites of temperature anomalies (Figs. 6a–d) reveal northeastward movement of significant cold air anomalies from midlatitudes into the Tropics during the surge period (from day −2 through day +2). Low-level circulation structures (Fig. 4) suggest that amplification of a band of cold air (negative anomalies) coincides with the enhancement of the southerly and southeasterly surge flow along the eastern flank of an anomalous anticyclone. As the midlatitude wave propagates eastward, the band of cold air is pushed toward the Tropics. At the time of the surge peak (day 0; Fig. 6b), the band of cold air is over the eastern Indian Ocean and prevails over the surge region. By day +2, a northwest–southeast-oriented cold front is established over the tropical and subtropical eastern Indian Ocean. After day +4, the northeastward movement terminates, and the cold anomaly weakens. Composite maps suggest that the coincident development of the cold front and southerlies characterizes an equatorward cold surge.

Specific humidity fields (Figs. 6e–h) show the formation of dry (negative) anomalies by the surge peak and the development of moist (positive) anomalies after that in the southerly surge region. By day 0, drying has approached the key region and a dry front has formed along the southerly and southeasterly surge (Fig. 4) over the tropical and subtropical eastern Indian Ocean. Here, a series of composite maps including day −1 phase (not shown) reveals that a weak preexisting dry anomaly in the key region mixes into the dry front. At the same time, a moist anomaly expands southward from north of the key region. From day +2 through day +4, a northwest–southeast elongated band of moist air anomalies prevails as the dry front erodes in the Tropics. This widespread moistening might produce convectively unstable conditions in the tropical eastern Indian Ocean region. This increase in low-level moisture may result from enhanced sea surface evaporation driven by increased surface winds in the southerly surge.

Maps of low-level temperature and humidity anomalies clearly depict the equatorward advection of cold and dry air in the southerly surge that originates in midlatitudes. Transport of midlatitude air into the Tropics during the surge is further confirmed by the behavior of PV anomalies on an isentropic surface using Lagrangian interpretation of airmass movement. Figure 7 shows the development of PV anomalies on the 315-K potential temperature surface from day −1 through day +2. This isentropic surface is in the middle to upper troposphere (500–200 hPa) at midlatitudes poleward of 30°S and in the midtroposphere (700–500 hPa) at low latitudes equatorward of 30°S during JJA (not shown).

The pattern of PV anomalies in midlatitudes is characterized by a well-defined wave train structure as in the circulation fields of Figs. 4 and 5. Recall that negative (positive) PV anomalies have cyclonic (anticyclonic) vorticity in the SH. The map sequence shows an anomalous PV trough extending toward the Tropics as the midlatitude wave propagates downstream. At day 0, a tongue of negative PV anomaly extends equatorward along the northeastern flank of the positive PV anomaly. At day +1, a streamer of negative PV anomaly oriented northwest-southeast stretches farther northwestward. On day +2, a PV anomaly of less than −0.03 PVU becomes cut off from the midlatitude wave train; this isolated cyclonic PV anomaly subsequently drifts westward around 20°S. Features in the PV evolution corroborate evidence of a midlatitude airmass intrusion into the lower latitudes.

b. Convectively unstable conditions in the Tropics

Surge-induced evaporation from the sea surface may be an important moisture source for the lower troposphere during the period between the surge peak and the convective peak. Composite lead–lag relationships of a variety of components will be compared to elucidate the roles of surge flow in preconditioning the convective environment. Figure 8 shows space–time structures of sea surface LHF and SHF anomalies presented in a similar way to the low-level temperature and moisture fields in Fig. 6. The evolution of LHF anomalies (Figs. 8a–d) shows that a positive LHF anomaly (evaporation) occurs coincident with the southerly surge core (Figs. 3 and 4) over the tropical and subtropical eastern Indian Ocean. The LHF in the surge region maximizes from day 0 through day +2, contributing to the local moisture accumulation preceding the convection (Figs. 6e–h). The SHF anomalies (Figs. 8e–

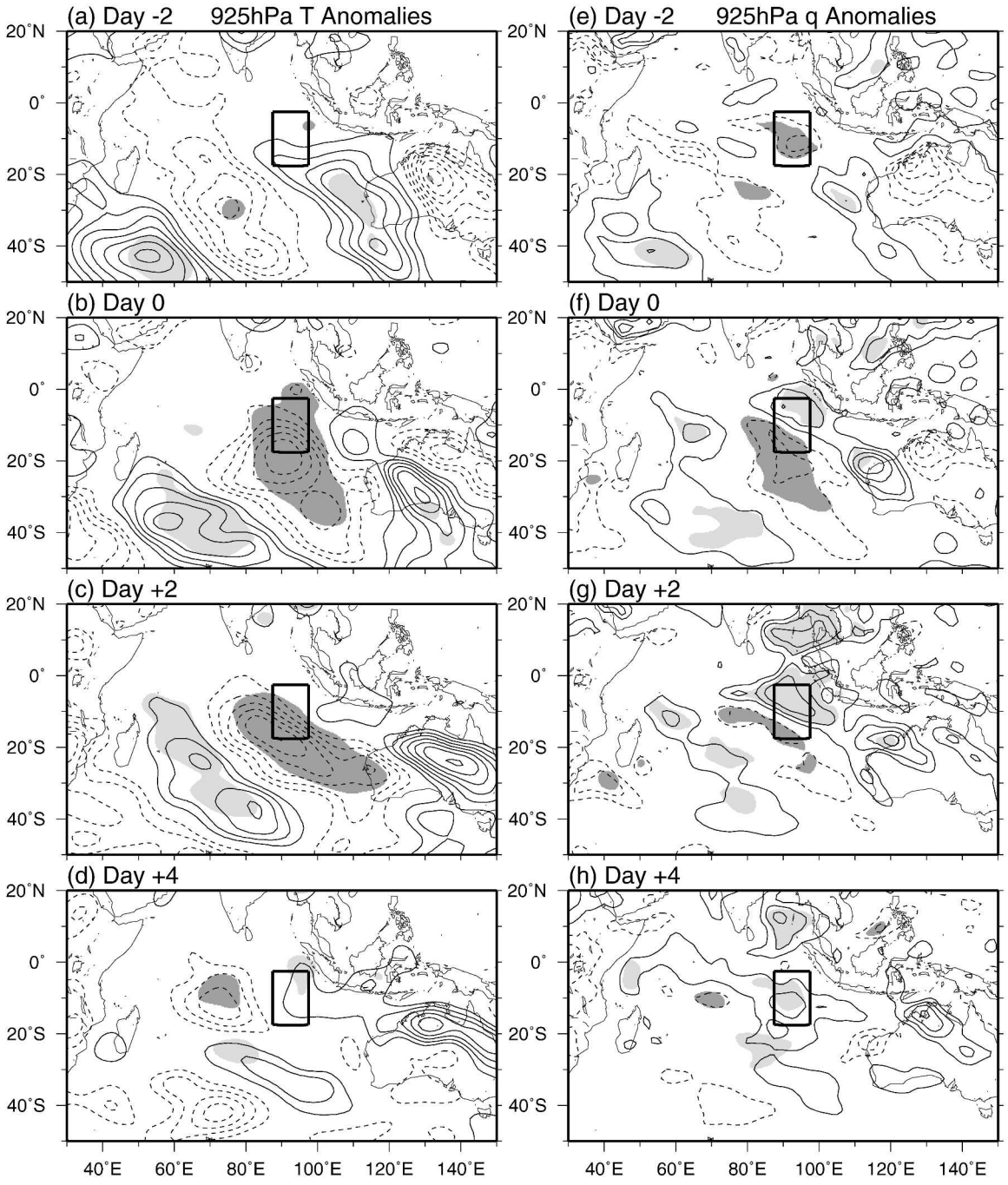

FIG. 6. (a)–(d) Composites of 925-hPa air temperature anomalies from day −2 through day +4 with 2-day interval based on the surge index. Solid (dashed) contours are positive (negative) values. Zero contours are omitted. Contour interval is 0.3 K. Negative (positive) anomalies statistically significant at the 99.9% level are darkly (lightly) shaded. (e)–(h) As in (a)–(d) but for 925-hPa specific humidity anomalies. Contour interval is 0.2 g kg^{-1}.

h) mimic the behavior of the LHF anomalies, but their magnitude is considerably smaller; thus, the SHF anomalies contribute less to the net surface heat budget. Strengthened surge winds, increased near-surface humidity deficit and air–sea temperature differences could enhance fluxes into the atmosphere during the surge period.

Finally, daily lag composites in the surge region were used to investigate the temporal phase relationship between the surge index (850-hPa v), OLR, moist static

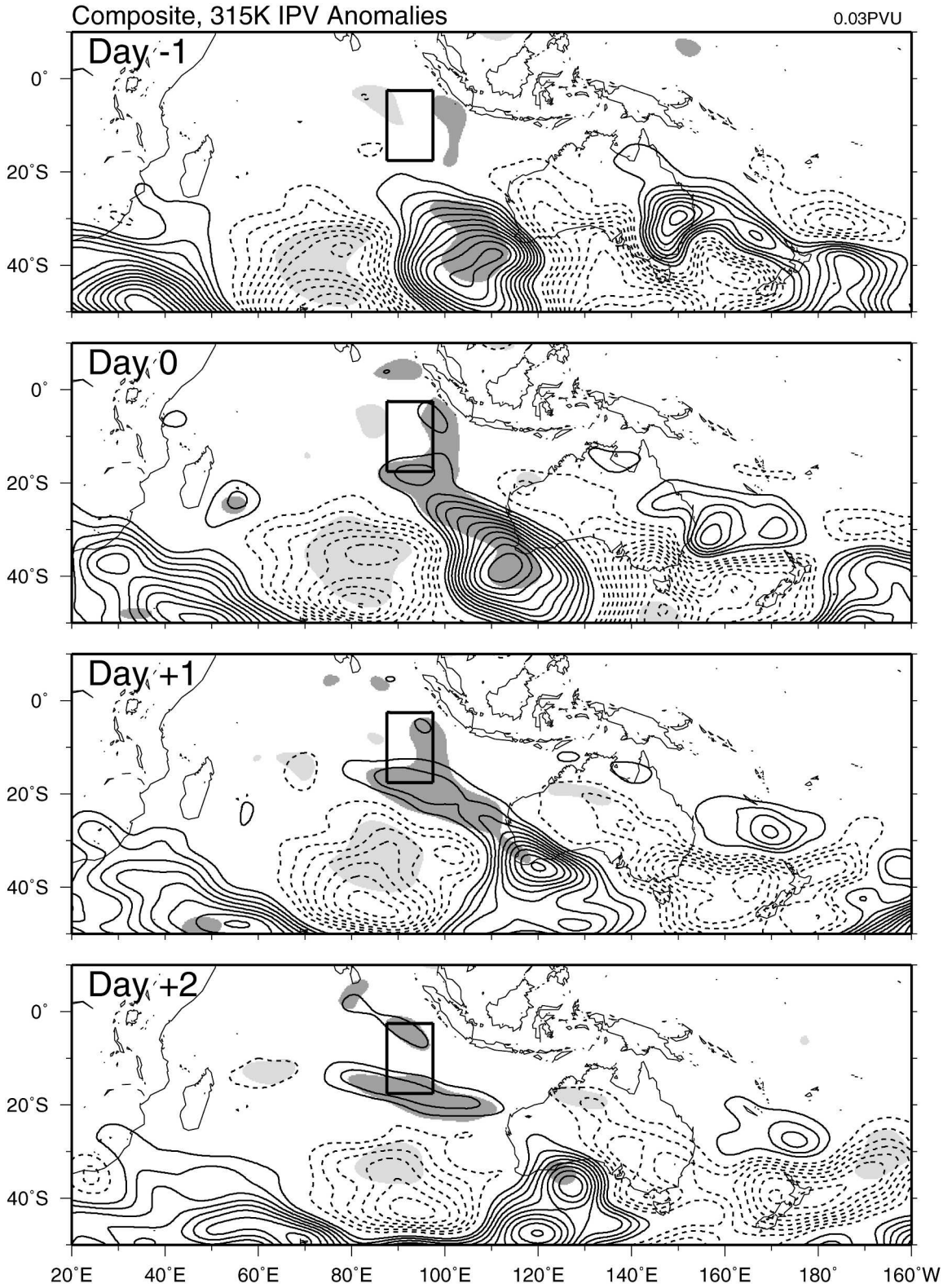

FIG. 7. Composites of isentropic PV (IPV) anomalies on the 315-K potential temperature surface from day −1 through day +2 with 1-day interval. Solid (dashed) contours are negative (positive) values. Zero contours are omitted. Contour interval is 0.03 PVU (10^{-6} K s^2 kg^{-1}). Negative (positive) anomalies statistically significant at the 99.9% level are darkly (lightly) shaded.

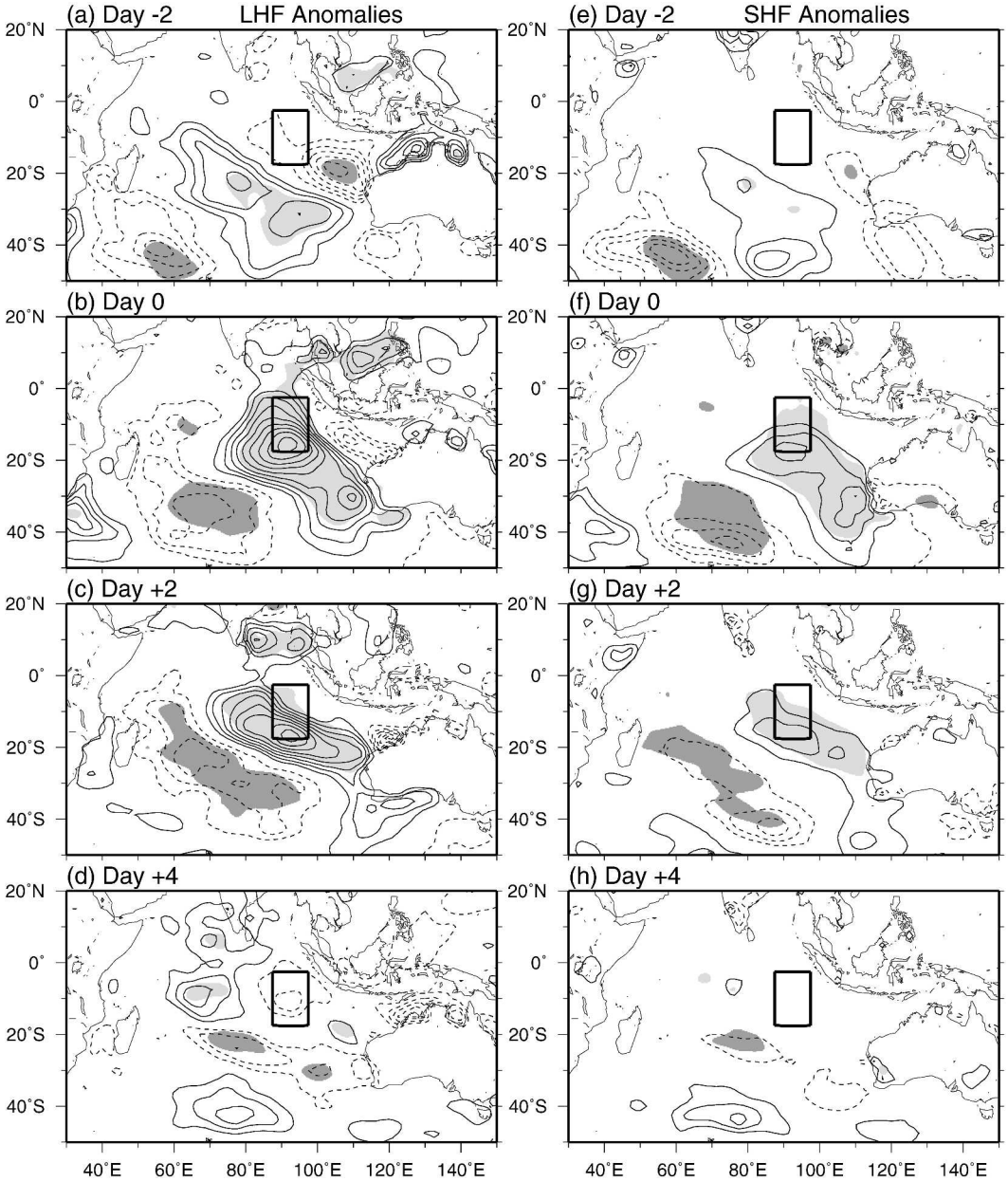

FIG. 8. (a)–(d) Composites of LHF anomalies from day −2 through day +4 with 2-day interval based on the surge index. Solid (dashed) contours are positive (negative) values. Zero contours are omitted. Contour interval is 20 W m^{-2}. Positive (negative) anomalies statistically significant at the 99.9% level are lightly (darkly) shaded. (e)–(h) As in (a)–(d) but for SHF anomalies. Contour interval is 5 W m^{-2}.

energy, instability index, low-level (850 hPa) divergence, and SLP. Moist static energy h is defined as $h = C_pT + gZ + Lq$, where C_p is the specific heat capacity of air, g is the gravitational acceleration, and L is the latent heat of condensation. The instability index is represented here as the difference in h between 925 and 700 hPa [h(925 hPa) − h (700 hPa)]. Kemball-Cook and Weare (2001) showed that this index is a useful measure of atmospheric stability. A positive index value represents convectively unstable atmospheric conditions. Figure 9 shows composite anomalies of the above variables averaged over a grid box (15°S–0°, 85°–100°E). This grid box well enclosing the tropical convective signal after the surge peak (Figs. 4 and 5) was used to construct composite time series of all variables except the surge index. Surge index and OLR time se-

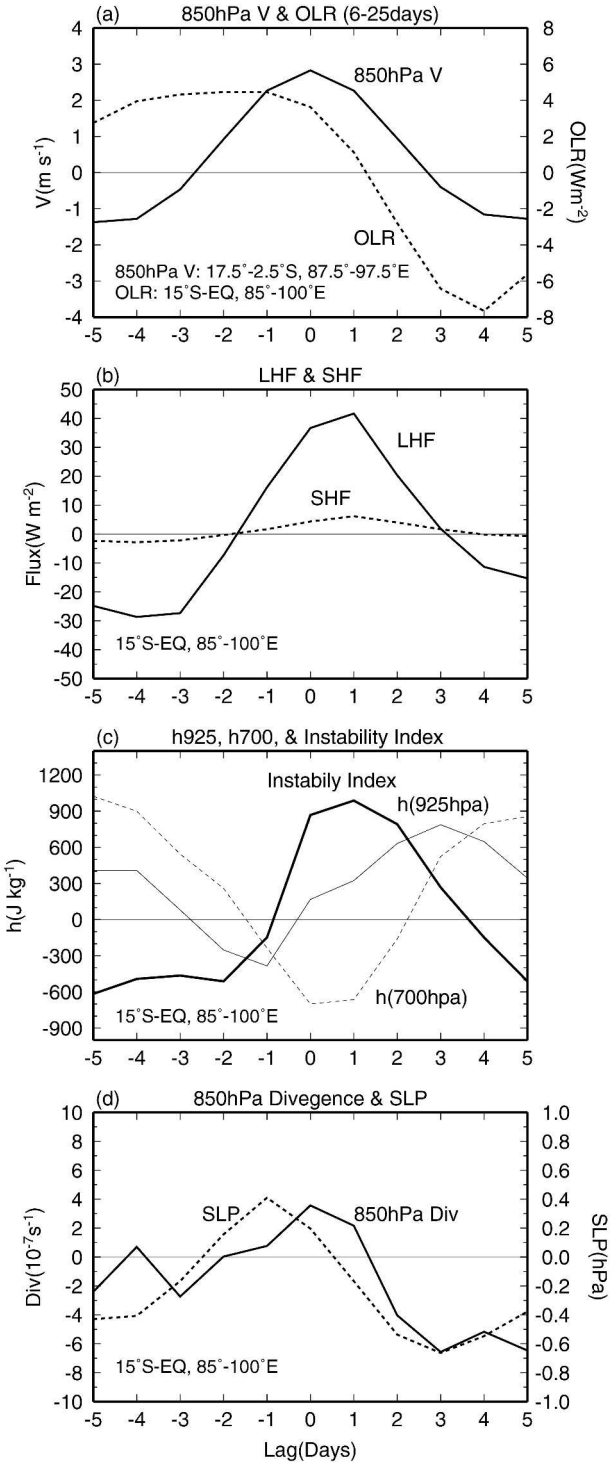

FIG. 9. (a) Composite evolution of 6–25-day filtered 850-hPa meridional wind (solid) and OLR (dashed) anomalies. OLR anomalies are averaged over the box 15°S–0°, 85°–100°E. (b) Composite evolution of LHF (solid) and SHF (dashed) anomalies over the same box with OLR anomalies. (c) As in (b) but for moist static energy anomalies at the 925- (thin solid) and 700-hPa (dashed) levels, and instability index (thick solid) anomalies. (d) As in (b) but for 850-hPa divergence (solid) and SLP (dashed) anomalies.

ries were bandpass filtered; all other variables were unfiltered except for removal of the annual cycle. It is noted here that if we use the same box with the surge key region for constructing composites of above variables, the temporal relationships among those basically do not change.

Composites of the surge index and the OLR anomaly (Fig. 9a) show the timing relationship between the southerly surge and subsequent convection. An OLR minimum, which can be regarded as a convective peak, occurs 3 to 4 days after the southerly surge peak (day 0). During the mature stage of the surge (day −1 to day +1), the LHF anomaly increases and reaches a positive peak at day +1 (Fig. 9b). The surge forces sea surface evaporation.

The SHF shows similar variability, but its contribution is small. Instability index changes (Fig. 9c) are roughly in phase with those of the surge index and the LHF, but with a 1-day lag. After a sharp increase from day −1 to day 0, instability is sustained from day 0 through day +2, with a peak at day +1. This local build up of instability followed by a surge is dominated by a rapid drop in h(700 hPa) and a gradual increase in h(925 hPa). During the mature stage of the surge, the rapid decrease of h(700 hPa) is linked to the mid–lower-tropospheric cold and dry air advection associated with the surge; 700-hPa T and q anomalies become negative at this time (not shown). A concurrent increase of h(925 hPa) (day 0 to day +2) is associated with the positive 925-hPa q anomaly shown in Figs. 6e–h. Initial moistening in the near-surface layer is driven by surge-linked evaporation and resulting transport of moisture into the convective region. Low-level convergence is not dominant during this period (Fig. 9d).

The 850-hPa divergence and SLP anomaly (Fig. 9d) imply strong convergence from day +2 through day +4, by which time instability is decreasing (Fig. 9c). However, the 925-hPa q continues to increase, reaching a maximum when the low-level convergence peaks. Thus, low-level convergence at this stage can increase near-surface q. The peak in convergence, however, occurs 2 days after the peak in instability, suggesting that low-level convergence is not responsible for the buildup of instability following the surge, but is linked directly to the subsequent convective signal captured by the OLR. Overall, the phase relationships among these variables highlight the crucial role played by the surge in creating the low-level instability prior to convection over the tropical eastern Indian Ocean. Low-level instability induced by the surge and the accompanying air–sea interaction can set the stage for subsequent tropical convection.

6. Discussion

Low-level meridional wind variance at submonthly time scales (Fig. 1a) shows that the tropical eastern Indian Ocean is a preferred region for equatorward surges. Factors that allow surge activity in this geographical location are important, but little is known about the cause of this geographical dependence. Major meridional surge activities typically occur near continental-scale mountain ranges such as the Tibetan Plateau of Asia, the Rockies of North America, and the Andes of South America (Garreaud 2001). Past studies have suggested that the prominent topography plays a crucial role in intensifying cold surges and determining the geographically fixed locations of surge activities downstream of the topography. Several studies recognized that dynamic interaction between midlatitude waves developing eastward and the large-scale topography drives low-level equatorward flow (e.g., Murakami and Sumi 1981; Hsu 1987; Murakami and Ho 1981; Garreaud 2000).

In contrast, oceanic surge activity in the present case does not depend on upstream large-scale topography; the basic atmospheric flow over the eastern Indian Ocean can produce surge activity despite the lack of topography. One essential feature that controls this preferred geographical location is the mean subtropical jet stream. As shown in sections 3 and 4, surge activity is north of the subtropical jet entrance region over the eastern Indian Ocean off the west coast of Australia in the SH winter. Present composite analyses suggest that the subtropical jet entrance region favors strong baroclinic development of Rossby waves that are carried eastward by the subtropical jet. Therefore, amplification of the wave within the jet entrance environment may cause the low-level surge, even in the absence of upstream topography.

We have emphasized that the presence of the wave activity along the SH subtropical westerly jet is responsible for the low-level meridional surge activity in the eastern Indian Ocean. However, the results presented here are derived based on only the SH winter (JJA) season. The seasonal dependence of the surge activity related to the location and strength of the subtropical jet was not examined, and that is open to discussion. As shown in Fig. 1 of Kiladis and Weickmann (1997), comparatively weaker subtropical jet exists also in the fall (March–May) and spring (September–November) seasons. Therefore, it seems reasonable to suppose that the similar type of tropical–extratropical connection is observed in this region during these seasons. In the summer (December–February) season, that may not be expected because of a lack of the subtropical jet. In addition, the primary wave propagation path in the SH midlatitude for the SH summer season (Hsu and Lin 1992) is different from that for the SH winter season (Ambrizzi et al. 1995). It calls for further investigation of the seasonal dependence of the surge activity for these other seasons.

As moist instability is released, low-level convergence increases until the convective maximum is reached in and around the surge key region. Increasing low-level convergence can further concentrate moisture and facilitate ascent and convective development. The mechanism that forces low-level convergence following the surge peak is still ambiguous. A trough feature east of the southeasterly surge flow in the SH equatorial Tropics (Fig. 4c; positive streamfunction values) may contribute to force initial low-level convergence. The development and westward extension of an apparent anomalous cyclone after the surge peak was confirmed in composites of SLP and 850-hPa z fields (not shown). This anomalous cyclone is likely an equatorially trapped wave signature in response to the surge. Once the initial low-level convergence induces ascending motion in convectively unstable conditions, convective processes in the low-level cyclonic environment may further promote subsequent growth of low-level convergence. One of the possibilities for causing the initial convergence after the surge peak may be boundary layer friction associated with the strengthened surge flow. Boundary layer frictional effect on the near-surface surge winds may result in the convergence in the boundary layer. Upward motion induced by the boundary layer frictional convergence further reinforces convergence in the lower free troposphere, and that may be capable of producing convection in the moist unstable condition. Diagnostic analysis of boundary layer flow applying the model of boundary layer motion (e.g., Wang and Li 1994) to our case using observational near-surface winds is needed for confirmation of this process.

Another important aspect of the surge is the transport of midlatitude dry air into the Tropics. The behavior of a cyclonic PV anomaly in the surge region (Fig. 7) implies an intrusion of dry air from the midlatitude midtroposphere into the tropical lower troposphere over the eastern Indian Ocean. One of the preferred locations for equatorward dry air intrusion events is the eastern Pacific westerly duct region during the NH winter. A strong equatorward extension of PV accompanied by Rossby wave propagation from the midlatitudes into the Tropics facilitates dry-air intrusion in this region (e.g., Kiladis and Weickmann 1992; Tomas and Webster 1994; Kiladis 1998; Waugh and Polvani 2000; Waugh and Funatsu 2003). Other studies have detected

the dry air intrusion and its potential effect on the tropical atmosphere over the Tropical Ocean Global Atmosphere Coupled Ocean–Atmosphere Experiment (TOGA COARE) domain of the western Pacific (e.g., Numaguti et al. 1995; Yoneyama and Fujitani 1995; Yoneyama and Parsons 1999; Parsons et al. 2000; Yoneyama 2003). Furthermore, Yatagai and Sumi (1998) noted that both the Pacific and Indian Oceans were locations for frequent dry air intrusions. However, few studies have addressed the role of dry air intrusions over the Indian Ocean.

We have been concerned with the possible impact of the low-level surge on the subsequent development of unstable atmospheric condition for convection in the eastern Indian Ocean. One good example that is comparable with the present result can be a case of the dry air intrusion event that occurred over the TOGA COARE domain in mid-November 1992. This event is treated in the TOGA COARE case studies (e.g., Numaguti et al. 1995; Ding et al. 1995; Yoneyama and Parsons 1999; Parsons et al. 2000). In this case, a dry air mass that originated in the SH subtropics moved into the equatorial western Pacific accompanied by strengthened low-level southerly flow. Based on this event, Parsons et al. (2000) proposed a conceptual model of a dry intrusion and the following development of convection. This model is constructed from consideration of atmospheric boundary layer dynamics and air–sea interaction. The brief description is as follows. An injection of dry air into the tropical middle and lower troposphere suppresses widespread convection because of decrease of buoyancy in boundary layer. Then boundary layer entrainment promotes downward transport of dry air and momentum, which leads to an increase of sea surface latent flux into the boundary layer. In turn, moistening of the boundary layer via the sea surface latent flux occurs. Furthermore, moistening of the lower troposphere aids in recharge of convective energy. The time for recovery from the extreme dry condition to the moist condition and the next convective organization is shorter than a week for this case (Fig. 20 of Parsons et al. 2000). It is possible that this sequence of local processes is applicable also to dry air intrusions over the eastern Indian Ocean. As evidenced in the previous section, a recovery of low-level moist unstable condition occurs within a week after the peak of the low-level surge and associated drying. Nevertheless, it would be difficult to confirm existence of the same boundary layer process from the present results. Because our composite results do not resolve air motion in the boundary layer, that is a limitation of this study. To confirm whether this conceptual model is applicable or not, dry air intrusions associated with low-level surges over the eastern Indian Ocean should be investigated in detail with case studies based on satellite and in situ observational data in the future.

7. Conclusions

This study investigated the large-scale characteristics of low-level southerly surges on submonthly time scales over the eastern Indian Ocean during the SH winter. The tropical and subtropical eastern Indian Ocean is a preferred region of cold surge activity at this high-frequency time scale. Composite analyses highlight the tropical–extratropical links associated with surges and surge impacts on the tropical atmosphere and give rise to discussions of surge-related atmospheric phenomenon.

Low-level southerly surges over the eastern Indian Ocean are caused by strong baroclinic development of midlatitude Rossby waves in the subtropical jet entrance region. The strengthened low-level winds constitute a cross-equatorial flow that stretches from the subtropical eastern Indian Ocean into the southern Bay of Bengal; this flow is confluent with the monsoon westerly flow. During the surge, a midlatitude wave train that is the origin of the surge extends from the southern Indian Ocean into the South Pacific. Midlatitude waves show a clear signature of downstream propagation and dispersion along the subtropical jet, suggesting that they are trapped within the SH winter waveguide. Surges that accompany wave passage force advection of cold and dry air from midlatitudes into the Tropics. The resulting development of a cold and dry front in the southerly surge is prominent during the surge period.

The low-level southerly surge associated with the midlatitude wave passage is an important source of tropical atmospheric variability over the eastern Indian Ocean. The subsequent organization of tropical convection 2–4 days after the surge peak is an important surge impact. The low-level surge forces advection of cold and dry air and subsequent near-surface moistening owing to the enhanced sea surface evaporation. This increases the instability in the surge region. Consequently, surge-induced moist instability acts as a trigger for the local flare up of subsequent convection.

The southerly surge on submonthly time scales is an important bridge that links midlatitudes and the Tropics over the Indian Ocean. Potential vorticity analyses suggest that the surge is manifested as an intrusion of dry air from the midlatitude midtroposphere into the tropical lower troposphere over the eastern Indian Ocean. Further studies exploring physical processes in the dry-air intrusion would facilitate an understanding of tropical–extratropical connections in this region.

Acknowledgments. The authors would like to thank three anonymous reviewers for valuable comments that helped to improve the quality of this paper. Both the NCEP–DOE AMIP II reanalysis and the NOAA OLR dataset were obtained from the NOAA/CDC (ftp://ftp.cdc.noaa.gov). The Generic Mapping Tools (GMT) graphics package outlined by Wessel and Smith (1995) was used for drawing all the figures.

REFERENCES

Adams, J. C., and P. N. Swarztrauber, 1999: SPHEREPACK 3.0: A model development facility. *Mon. Wea. Rev.,* **127,** 1872–1878.

Ambrizzi, T., B. J. Hoskins, and H.-H. Hsu, 1995: Rossby wave propagation and teleconnection patterns in the austral winter. *J. Atmos. Sci.,* **52,** 3661–3672.

Carrera, M. L., and J. R. Gyakum, 2003: Significant events of interhemispheric atmospheric mass exchange: Composite structure and evolution. *J. Climate,* **16,** 4061–4078.

Compo, G. P., G. N. Kiladis, and P. J. Webster, 1999: The horizontal and vertical structure of east Asian winter monsoon pressure surges. *Quart. J. Roy. Meteor. Soc.,* **125,** 29–54.

Ding, Y.-H., A. Sumi, and X. S. Shen, 1995: Structures of the mixed layer and estimates of sea surface fluxes during TOGA COARE IOP. *J. Meteor. Soc. Japan,* **73,** 569–583.

Fukutomi, Y., and T. Yasunari, 1999: 10–25-day intraseasonal variations of convection and circulation over east Asia and western North Pacific during early summer. *J. Meteor. Soc. Japan,* **77,** 753–769.

——, and ——, 2002: Tropical–extratropical interaction associated with the 10–25-day oscillation over the western Pacific during the northern summer. *J. Meteor. Soc. Japan,* **80,** 311–331.

Garreaud, R. D., 2000: Cold air incursions over subtropical South America: Mean structure and dynamics. *Mon. Wea. Rev.,* **128,** 2544–2559.

——, 2001: Subtropical cold surges: Regional aspects and global distribution. *Int. J. Climatol.,* **21,** 1181–1197.

——, and J. M. Wallace, 1998: Summertime incursions of midlatitude air into subtropical and tropical South America. *Mon. Wea. Rev.,* **126,** 2713–2733.

Hsu, H.-H., 1987: Propagation of low-level circulation features in the vicinity of mountain ranges. *Mon. Wea. Rev.,* **115,** 1864–1893.

——, and S.-H. Lin, 1992: Global teleconnections in the 250-mb streamfunction field during the Northern Hemisphere winter. *Mon. Wea. Rev.,* **120,** 1169–1190.

Kanamitsu, M., W. Ebisuzaki, J. Woollen, S.-K. Yang, J. J. Hnilo, M. Fiorino, and G. L. Potter, 2002: NCEP–DOE AMIP-II Reanalysis (R2). *Bull. Amer. Meteor. Soc.,* **83,** 1631–1643.

Kaylor, R. E., 1977: Filtering and decimation of digital time series. Institute of Physical Science Technology Tech. Note BN 850, University of Maryland, College Park, 42 pp.

Kemball-Cook, S. R., and B. C. Weare, 2001: The onset of convection in the Madden–Julian oscillation. *J. Climate,* **14,** 780–793.

Kiladis, G. N., 1998: Observations of Rossby waves linked to convection over the eastern tropical Pacific. *J. Atmos. Sci.,* **55,** 321–339.

——, and K. M. Weickmann, 1992: Extratropical forcing of tropical convection during northern winter. *Mon. Wea. Rev.,* **120,** 1924–1938.

——, and ——, 1997: Horizontal structure and seasonality of large-scale circulations associated with submonthly tropical convection. *Mon. Wea. Rev.,* **125,** 1997–2013.

——, and K. C. Mo, 1999: Interannual and intraseasonal variability in the Southern Hemisphere. *Meteorology of the Southern Hemisphere, Meteor. Monogr.,* No. 49, Amer. Meteor. Soc., 307–336.

——, G. A. Meehl, and K. M. Weickmann, 1994: Large-scale circulation associated with westerly wind bursts and deep convection over the western equatorial Pacific. *J. Geophys. Res.,* **99,** 18 527–18 544.

Liebmann, B., G. N. Kiladis, J. A. Marengo, T. Ambrizzi, and J. D. Glick, 1999: Submonthly convective variability over South America and the South Atlantic convergence zone. *J. Climate,* **12,** 1877–1891.

Madden, R. A., and P. R. Julian, 1994: Observations of the 40–50-day tropical oscillation: A review. *Mon. Wea. Rev.,* **122,** 814–837.

Marengo, J. A., T. Ambrizzi, G. Kiladis, and B. Liebmann, 2002: Upper-air wave trains over the Pacific Ocean and wintertime cold surges in tropical–subtropical South America leading to freezes in southern and southeastern Brazil. *Theor. Appl. Climatol.,* **73,** 223–242.

Matthews, A. J., and G. N. Kiladis, 1999: The tropical–extratropical interaction between high-frequency transients and the Madden–Julian oscillation. *Mon. Wea. Rev.,* **127,** 661–677.

Meehl, G. A., G. N. Kiladis, K. M. Weickmann, M. Wheeler, D. S. Gutzler, and G. P. Compo, 1996: Modulation of equatorial subseasonal convective episodes by tropical–extratropical interaction in the Indian and Pacific Ocean regions. *J. Geophys. Res.,* **101,** 15 033–15 049.

Murakami, T., 1987: Intraseasonal atmospheric teleconnection patterns during the Northern Hemisphere summer. *Mon. Wea. Rev.,* **115,** 2133–2154.

——, 1988a: Intraseasonal atmospheric teleconnection patterns during the Northern Hemisphere winter. *J. Climate,* **1,** 117–131.

——, 1988b: Equatorward surges, equatorial westerlies and convection on interannual and intraseasonal time scales. UHMET88-02, Department of Meteorology, University of Hawaii, Honolulu, HI, 18 pp.

——, and L. Y. C. Ho, 1981: Orographic influence of the Rocky Mountains on the winter circulation over contiguous United States. Part II: Synoptic-scale (short-period) disturbances. *J. Meteor. Soc. Japan,* **59,** 646–671.

——, and A. Sumi, 1981: Large-scale aspects of the 1978–79 winter circulation over the greater WMONEX region. Part II: Long-period perturbations. *J. Meteor. Soc. Japan,* **59,** 646–671.

——, and W. L. Sumathipala, 1989: Westerly bursts during the 1982/83 ENSO. *J. Climate,* **2,** 71–85.

Numaguti, A., R. Oki, K. Nakamura, K. Tsuboki, N. Misawa, T. Asai, and Y.-M. Kodama, 1995: 4–5-day-period variation and low-level dry air observed in the equatorial western Pacific during the TOGA COARE IOP. *J. Meteor. Soc. Japan,* **73,** 267–290.

Pan, H.-L., and F.-X. Zhou, 1985: The 10–20 day tropical–midlatitude interactions during the winter monsoon season. *J. Meteor. Soc. Japan,* **63,** 829–844.

Parsons, J. M., K. Yoneyama, and J.-L. Redelsperger, 2000: The

evolution of the tropical western Pacific atmosphere–ocean system following the arrival of a dry intrusion. *Quart. J. Roy. Meteor. Soc.,* **126,** 517–548.

Rodwell, M. J., 1997: Breaks in the Asian monsoon: The influence of Southern Hemisphere weather systems. *J. Atmos. Sci.,* **54,** 2597–2611.

Schrage, J. M., and D. G. Vincent, 1996: Tropical convection on 7–21-day timescales over the western Pacific. *J. Climate,* **9,** 587–607.

Shrestha, M. L., and T. Murakami, 1988: Intraseasonal fluctuations in low-level meridional winds over the Indian Ocean and monsoonal convection over south Asia. *Tellus,* **40A,** 120–132.

Slingo, J. M., 1998: Extratropical forcing of tropical convection in a northern winter simulation with the UGAMP GCM. *Quart. J. Roy. Meteor. Soc.,* **124,** 27–51.

Tomas, R. A., and P. J. Webster, 1994: Horizontal and vertical structure of cross-equatorial wave propagation. *J. Atmos. Sci.,* **51,** 1417–1430.

Vincent, D. G., A. Fink, J. M. Schrage, and P. Speth, 1998: High- and low-frequency intraseasonal variance of OLR on annual and ENSO timescales. *J. Climate,* **11,** 968–986.

Wang, B., and T. Li, 1994: Convective interaction with boundary-layer dynamics in the development of a tropical intraseasonal system. *J. Atmos. Sci.,* **51,** 1386–1400.

Wang, X.-L., and T. Murakami, 1987: Intraseasonal meridional surges and equatorial convections during the Southern Hemisphere summer. *J. Meteor. Soc. Japan,* **65,** 727–736.

Waugh, D. W., and L. M. Polvani, 2000: Climatology of intrusions into the tropical upper troposphere. *Geophys. Res. Lett.,* **27,** 3857–3860.

——, and B. M. Funatsu, 2003: Intrusions into the tropical upper troposphere: Three-dimensional structure and accompanying ozone and OLR distributions. *J. Atmos. Sci.,* **60,** 637–653.

Wessel, P., and W. H. F. Smith, 1995: New version of the Generic Mapping Tools released. *Eos, Trans. Amer. Geophys. Union,* **76,** 329.

Yasunari, T., 1981a: Structure of an Indian summer monsoon system with around 40-day period. *J. Meteor. Soc. Japan,* **59,** 336–354.

——, 1981b: Influence of the Southern Hemisphere circulations on the active-break cycle of the Indian summer monsoon. *Proc. Third Symp. on Polar Meteorology and Glaciology,* Tokyo, Japan, National Institute of Polar Research, 223–233.

Yatagai, A., and A. Sumi, 1998: Statistical features of dry air intrusions into the equatorial ocean. *Proc. COARE 98*, Boulder, CO, CLIVAR/GEWEX, WCRP-107, WMO Tech. Doc. 940, 161–162.

Yoneyama, K., 2003: Moisture variability over the tropical western Pacific Ocean. *J. Meteor. Soc. Japan,* **81,** 317–337.

——, and T. Fujitani, 1995: The behavior of dry westerly air associated with convection during the TOGA-COARE R/V Natsusima cruise. *J. Meteor. Soc. Japan,* **73,** 291–304.

——, and D. B. Parsons, 1999: A proposed mechanism for the intrusion of dry air into the tropical western Pacific region. *J. Atmos. Sci.,* **56,** 1524–1546.